Characterization of $Na_5P_3O_{10}$ Polymorphs by ^{23}Na MAS, ^{23}Na MQMAS, and ^{31}P MAS NMR Spectroscopy

Colin A. Fyfe,* Holger Meyer zu Altenschildesche, and Jørgen Skibsted

Department of Chemistry, University of British Columbia, 2036 Main Mall, Vancouver B.C., Canada V6T 1Z1

Received May 8, 1998

The two anhydrous polymorphs of $Na_5P_3O_{10}$ have been characterized by ^{23}Na and ^{31}P MAS NMR spectroscopy. The ^{23}Na multiple-quantum (MQ) MAS NMR spectrum of the low-temperature form (phase II) displays three resonances for which the quadrupole coupling parameters and isotropic chemical shifts have been accurately determined from the MAS NMR spectra of the central transition. Thereby, discrepancies between recently reported ^{23}Na MQMAS spectra of this phase and the crystal structure have been clarified. The ^{23}Na resonances observed for the low-temperature form are assigned to the crystallographically nonequivalent Na sites in the crystal structure using point-monopole calculations of the electric-field gradient tensors. Three ^{23}Na resonances have also been observed for the high-temperature form (phase I), with two signals having very similar quadrupolar couplings and isotropic chemical shifts indicating similar coordination environments for the corresponding Na sites, in disagreement with the reported single-crystal structure. Point-monopole calculations of the electric-field gradient tensors based on the crystal structure fail to reproduce the experimental values. The ^{31}P chemical shielding anisotropies, obtained from ^{31}P MAS NMR spectra, show that the terminal P atoms of the $P_3O_{10}^{5-}$ ions have a negative shielding anisotropy parameter ($\delta_\sigma = \delta_{iso} - \delta_{33}$) in agreement with similar observations reported for diphosphates. This characteristic feature has been used in the assignment of the three ^{31}P resonances observed for the hexahydrate $Na_5P_3O_{10}\cdot 6H_2O$.

Introduction

Pentasodium triphosphate, $Na_5P_3O_{10}$, is one of the main products made from phosphoric acid.[1] In the 1940s it was introduced as a builder for synthetic detergents, and in 1970 its production in the U.S.A. alone topped 1 million metric tons per year. Due to changed environmental regulations and the following substitution of sodium triphosphate by other compounds (e.g. zeolites) in most household laundry detergents, production has significantly decreased since then. However, $Na_5P_3O_{10}$ is still widely used in automatic dishwashing formulations, industrial cleaners, car washes and various industrial applications. Thus, it remains one of the commercially most significant phosphorus compounds.[2]

$Na_5P_3O_{10}$ crystallizes in two anhydrous polymorphic forms of which the low-temperature polymorph (phase II) is thermodynamically stable up to about 415 °C.[3,4] At higher temperatures it is easily converted to the high-temperature polymorph (phase I). Since the reverse process is very slow, phase I is metastable at room-temperature and both polymorphs can coexist. Depending on its thermal history and technical grade, $Na_5P_3O_{10}$ is usually a mixture containing varying amounts of the two phases. From aqueous solutions pentasodium triphosphate crystallizes as the hexahydrate, $Na_5P_3O_{10}\cdot 6H_2O$. Hydration of anhydrous $Na_5P_3O_{10}$ from air, however, occurs only slowly and at high relative humidities.

The coexistence of three different crystalline forms under ambient conditions presents a challenge for technical applications since the physical properties of the three phases are very different. For example, phase I hydrates much faster than phase II, forming crystals of the hexahydrate which then determine the solubility. On the other hand, the overall solubility of phase II is much greater than that for phase I, and highly supersaturated solutions can be obtained.[1] Obviously, these properties have important implications in many industrial applications and a large number of investigations have been devoted to their understanding.[3,4]

Because X-ray diffraction (XRD) directly reflects the crystal structure, such techniques are probably the most widely used methods to investigate and distinguish different crystalline forms of substances. However, since only one polymorph is thermodynamically stable under a given set of environmental conditions, it is often impossible to obtain crystals of suitable size and quality for straightforward single-crystal structure analysis. In this case, one has to resort to powder XRD techniques where the overlap of reflections limits the information content.[5,6] Other important analytical tools include optical and electron microscopy, thermal analysis (e.g. calorimetry, DTA, DSC, and TGA), IR, and solid-state NMR spectroscopy. Solid-state NMR is particularly useful since it directly reflects the local environment of the nucleus under investigation.[7−10] Thus, NMR interaction parameters can be correlated with structural features such as

(1) *Kirk−Othmer Encyclopedia of Chemical Technology*, 4th ed.; John Wiley & Sons: New York, 1996; Vol. 18, p 699.
(2) *Ullmann's Encyclopedia of Industrial Chemistry*, 5th ed.; VCH: Weinheim, 1991; Vol. A19, p 488.
(3) Durif, A. *Crystal Chemistry of Condensed Phosphates*; Plenum Press: New York, 1995.
(4) Averbuch-Pouchot, M.-T.; Durif, A. *Topics in Phosphate Chemistry*; World Scientific: Singapore, 1996.
(5) Young, R. A. *The Rietveld Method*; Oxford University Press: Oxford, 1993.
(6) McCusker, L. B. *Acta Crystallogr.* **1991**, *A47*, 297.
(7) Fyfe, C. A. *Solid State NMR for Chemists*; CFC Press: Guelph, 1983.

10.1021/ic980524o CCC: $18.00
Published on Web 12/11/1998

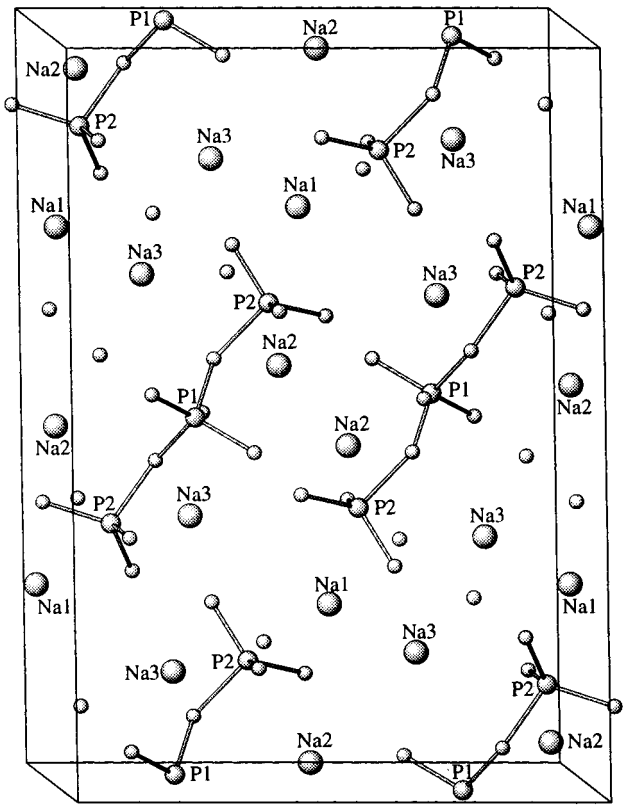

Figure 1. Perspective diagram of the monoclinic unit cell for the low-temperature form of $Na_5P_3O_{10}$ (phase II) based on the data from the reported single-crystal structure.[11] The unit cell contains four units of $Na_5P_3O_{10}$ and its dimensions are $a = 16.00$ Å, $b = 5.24$ Å, $c = 11.25$ Å, and $\beta = 93°$. For clarity, the indices of the oxygen atoms are not shown and only the P−O bonds are included to illustrate the presence of the linear $P_3O_{10}^{5-}$ units.

local subunits, bond distances and angles, or coordination geometries. Furthermore, the intensities of NMR signals are proportional to the number of atoms per unit cell, and relative occupancies of different atomic sites can be determined.

The structures of the two anhydrous polymorphs of $Na_5P_3O_{10}$ were determined in the late 1950s by single-crystal XRD.[11−13] Both polymorphs crystallize in the monoclinic space group *C*2/*c* with four formula units per unit cell. The structures are composed of sodium cations and linear $P_3O_{10}^{5-}$ ions as illustrated for the low-temperature form in Figure 1. The central phosphorus atoms of the triphosphate groups lie on 2-fold axes and there are three different sodium sites in each of the structures, one of which occupies a center of symmetry. Thus, in both structures there are two phosphorus sites in a 1:2 ratio and three sodium sites in a 1:2:2 ratio.

The three-dimensional arrangement of the triphosphate group and the sodium cations, however, is very different for the two polymorphs resulting in quite different coordinations of the cations. In the low-temperature phase II all cations are surrounded by oxygen atoms in distorted octahedral arrangements[11] while in the high-temperature phase I this is only the case for two cationic sites.[12] The third sodium site in phase I possesses a very unusual 4-fold coordination, with all four oxygen atoms positioned on one side of the sodium atom and only very long Na−O contacts (>3 Å) on the other side. This unique environment has been used to explain the greater ease of hydration of phase I compared to phase II.[12] However, the author of the original single-crystal study mentions that the accuracy of the structure determination was limited by the poor quality of the crystals and by experimental problems.[12] In light of these remarks it is questionable whether such an extremely distorted and unusual cation coordination really exists in $Na_5P_3O_{10}$ (phase I).

The hexahydrate, $Na_5P_3O_{10}\cdot 6H_2O$, crystallizes in the triclinic space group $P\bar{1}$ with two formula units per unit cell.[14] All atoms lie on general positions, and thus there are three independent phosphorus and five sodium sites with equal multiplicities. The conformation of the triphosphate anion is very similar to those in the two anhydrous polymorphs. The water molecules are distributed in such a way that they partially coordinate the sodium ions and form hydrogen bonds to the triphosphate ion. One terminal PO_4 tetrahedron participates in nine such hydrogen bonds and the other only in one, while the central PO_4 tetrahedron does not take part in hydrogen bonding at all.[14]

$Na_5P_3O_{10}$ has been the focus of two recent ^{23}Na solid-state NMR investigations.[15,16] However, commercially available samples were used in these studies and the results were not in agreement with the crystal structures of any known polymorph. In particular, only two signals were observed in ^{23}Na multiple-quantum (MQ) MAS experiments and in one of the investigations[15] a 1:3 intensity ratio was employed for the simulation of the ^{23}Na MAS spectrum. In neither of the studies was any additional characterization performed to test if the samples were pure or presented mixtures of different phases.

In this work we have characterized the two different crystalline forms of sodium triphosphate using ^{23}Na and ^{31}P solid-state NMR techniques. This includes (i) a determination of ^{23}Na quadrupole coupling parameters and isotropic chemical shifts from ^{23}Na MAS and MQMAS spectra and (ii) a determination of the ^{31}P isotropic and anisotropic chemical shielding parameters for the two anhydrous forms and the hexahydrate from ^{31}P MAS NMR spectra. All NMR data are discussed in terms of the crystal structure data, and most of the ^{23}Na and ^{31}P NMR resonances can be unambiguously assigned to atom sites in the crystal structures. Inconsistencies between the ^{23}Na quadrupolar couplings determined here for phase I and its published structure suggest that a crystallographic re-evaluation of the sodium coordination environment in phase I should be performed.

Experimental Section

The solid-state ^{23}Na and ^{31}P MAS NMR experiments were performed at 9.4 and 11.7 T on Bruker MSL-400 and AMX-500 spectrometers using home-built, double-tuned $^{31}P/^{23}Na$ MAS (MSL-400) and single-tuned, narrow-bore MAS (AMX-500) probes, both equipped with a commercially available 5-mm spinner system (Doty Scientific Inc.) allowing spinning speeds up to 15 kHz to be employed. The wide-bore probe for the MSL-400 spectrometer included a single set of gradient coils which were used for the ^{23}Na pulsed field gradient (PFG) MQMAS experiments. The design of this probe has recently been described elsewhere.[17] The gradient pulses were obtained from a Bruker microimaging unit interfaced to the MSL-400 spectrometer and had a

(8) Engelhardt, G. Michel, D. *High-Resolution Solid-State NMR of Silicates and Zeolites*; Wiley: Chichester, 1987.
(9) Granger, P.; Harris, R. K. (Eds.) *Multinuclear Magnetic Resonance in Liquids and Solids: Chemical Applications*; Kluwer: Dordrecht, The Netherlands, 1990.
(10) Bell, A. T.; Pines, A. (Eds.) *NMR Techniques in Catalysis*; Marcel Dekker: New York, 1994.
(11) Davies, D. R.; Corbridge, D. E. C. *Acta Crystallogr.* **1958**, *11*, 315.
(12) Corbridge, D. E. C. *Acta Crystallogr.* **1960**, *13*, 263.
(13) Cruickshank, D. W. J. *Acta Crystallogr.* **1964**, *17*, 674.
(14) Wiench, D. M.; Jansen, M.; Hoppe, R. *Z. Anorg. Allg. Chem.* **1982**, *488*, 80.
(15) Medek, A.; Harwood: J. S.; Frydman, L. *J. Am. Chem. Soc.* **1995**, *117*, 12779.
(16) Hanaya, M.; Harris, R. K. *J. Phys. Chem. A* **1997**, *101*, 6903.

maximum gradient strength of approximately 60 G/cm. The ^{23}Na MAS and MQMAS NMR spectra were recorded using rf fields of 35 and 60 kHz at 11.7 and 9.4 T, respectively, while the ^{31}P MAS NMR experiments (9.4 T) employed an rf field strength of 42 kHz and a pulse duration of 3 μs. ^{23}Na and ^{31}P chemical shifts are reported relative to an aqueous 1.0 M NaCl solution and 85% H_3PO_4, respectively. The simulations of the ^{23}Na central transitions and of the ^{31}P spinning sideband manifolds were performed using programs described elsewhere.[18,19] For the ^{23}Na MAS NMR spectra the program considers the average Hamiltonian for the second-order quadrupolar interaction and includes intensities from the centerband as well as the spinning sidebands from the central transition.

Commercial samples of anhydrous $Na_5P_3O_{10}$ from two different manufacturers (Aldrich Chemicals and Alfa Products, technical purity grades) were initially characterized by ^{23}Na MAS NMR and powder XRD which revealed that both samples represented mixtures of the two $Na_5P_3O_{10}$ polymorphs. Pure samples of both phases were obtained from the hexahydrate ($Na_5P_3O_{10}\cdot 6H_2O$) which was prepared by slow evaporation of a concentrated aqueous solution of $Na_5P_3O_{10}$. After crystals had formed these were filtered from the solution, washed with acetone, and dried in air at room temperature. The low-temperature form was obtained by heating the hexahydrate at 200 °C for 4 days. The high-temperature form was prepared by heating the low-temperature form to 550 °C for 1 day, then slowly cooling the solid to 430 °C over a period of 12 h, and quenching the sample in liquid nitrogen. The purities of the two anhydrous polymorphs and of the hexahydrate were confirmed by comparing their powder X-ray diffraction patterns with the corresponding JCPDS files.

Results and Discussion

^{23}Na and ^{31}P NMR spectroscopies are very useful tools for determination of the numbers of nonequivalent ^{23}Na and ^{31}P sites and their relative occupancies. Further information may be gained from the anisotropic NMR parameters characterizing the ^{23}Na quadrupole coupling interaction (i.e. C_Q and η_Q) and the ^{31}P chemical shielding anisotropy tensors (i.e. δ_σ and η_σ) in addition to the ^{23}Na and ^{31}P isotropic chemical shifts. The first part of this section describes ^{23}Na MAS and MQMAS NMR spectra for the anhydrous pentasodium triphosphate phases and the assignment of the ^{23}Na quadrupole coupling parameters, obtained from these spectra, to the sodium sites in the crystal structures. The following part includes a determination of the ^{31}P CSA parameters for the two anhydrous phases and the hexahydrate and discusses the relationship of these parameters to structural sites and bonding geometries.

The ^{23}Na MQMAS NMR spectra were recorded using the recently introduced PFG-MQMAS method which utilizes pulsed field gradients (PFGs) for selection of the $p = -3$ and $p = -1$ coherence transfer pathway in the MQMAS experiment.[17] This has the advantage that no phase cycling of the rf pulses and the receiver needs to be employed, which may be of significant importance for extensions of the MQMAS sequence to include a magnetization transfer step to a heteronucleus. The pulse sequence, used in this work and shown in Figure 2, combines PFGs to select the $p = -3$ and $p = -1$ coherence transfer pathway with a pulse scheme which utilizes the rotation-induced adiabatic coherence transfer (RIACT)[20] that occurs between 3Q and central transition (1Q) coherences for spin $I = {}^3/_2$ nuclei. The RIACT method is chosen since this excitation/conversion scheme is expected to be less sensitive to variations in the magnitude of the quadrupolar interactions compared to the two- or three-pulse sequences[20] conventionally used.

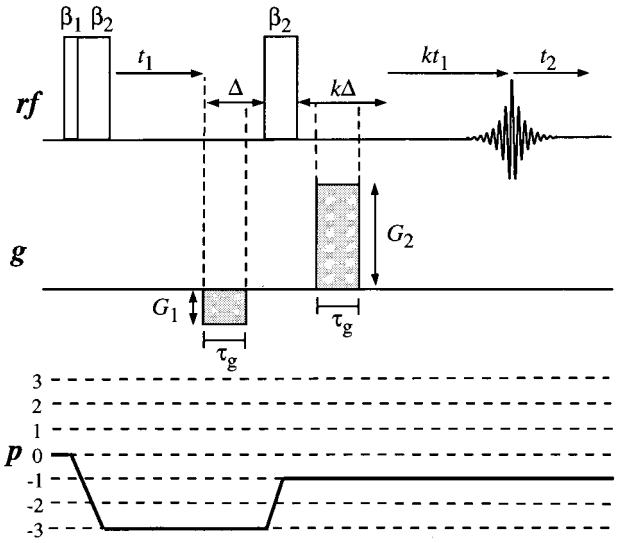

Figure 2. Radio frequency (rf) and gradient (g) pulse schemes for the PFG-MQMAS experiment selecting the $p = 0 \rightarrow -3 \rightarrow -1$ coherence transfer pathway for an $I = {}^3/_2$ spin nucleus. The fixed time Δ includes a gradient ring-down delay in addition to the gradient time (τ_g). For simplicity the acquisition begins at the top of the triple-quantum echo which is observed at kt_1, where $k = {}^7/_9$ for a spin-$^3/_2$ nucleus.[23,44] The phase of the first pulse (β_1) is shifted by 90° relative to the two spin-lock pulses (β_2). Otherwise no phase cycling of the pulses and the receiver is employed. The first pulse is set to a 90° liquid pulse while the spin-lock pulses have a length of approximately $4/\nu_r$.[20]

The ^{23}Na PFG-MQMAS NMR spectrum of the low-temperature form of $Na_5P_3O_{10}$ (phase II) illustrated in Figure 3 shows the presence of three structurally different Na sites. The 2D spectrum also displays a weak tilted line shape at the center of the F_1 dimension which is ascribed to single-quantum coherence that has not been completely dephased by the pulsed-field gradients. The ^{23}Na resonances at 9 and 46 ppm in the F_1 dimension have intensities which are considerably larger than that of the third one. Moreover, the 3Q resonance with low intensity is shifted to higher frequency in the F_1 dimension compared to the other ^{23}Na resonances which reflects a larger quadrupole coupling than that of the other two sites (assuming that the three Na sites have similar isotropic chemical shifts). It is well-known that MQMAS NMR experiments suffer from a reduced excitation efficiency of 3Q coherences for structural sites having strong quadrupolar interactions. Thus, the reduced intensity observed for the high-field signal in the 3Q dimension may reflect a very strong quadrupole coupling and/or a lower relative multiplicity for this site compared to the two other Na sites in the unit cell of $Na_5P_3O_{10}$ (II).

High-speed ^{23}Na MAS NMR spectra of the central transition for $Na_5P_3O_{10}$ (II) at 11.7 and 9.4 T are shown in Figure 4a and c, respectively. Both spectra exhibit features which can be associated with overlapping second-order quadrupolar line shapes from three Na sites. Most remarkable is the observation of the low-frequency singularity at −39 ppm, the shoulder at −54 ppm, and the edge at −73 ppm at 11.7 T (Figure 4a) which originate from a ^{23}Na site with a considerably larger quadrupole coupling compared to the two sites having second-order quadrupolar line shapes ranging from approximately 10 to −40 ppm. Simulations of the central transitions at 11.7 and 9.4 T are shown in Figure 4b and d, respectively, and correspond to the C_Q, η_Q, and δ_{iso} values for the three Na sites in $Na_5P_3O_{10}$

(17) Fyfe, C. A.; Skibsted, J.; Grondey, H.; Meyer zu Altenschildesche, H. *Chem. Phys. Lett.* **1997**, *281*, 44.
(18) Skibsted, J.; Bildsøe, H.; Jakobsen, H. J. *J. Magn. Reson.* **1991**, *92*, 669.
(19) Skibsted, J.; Nielsen, N. C.; Bildsøe, H.; Jakobsen, H. J. *J. Magn. Reson.* **1991**, *95*, 88.
(20) Wu, G.; Rovnyak, D.; Griffin, R. G. *J. Am. Chem. Soc.* **1996**, *118*, 9326.

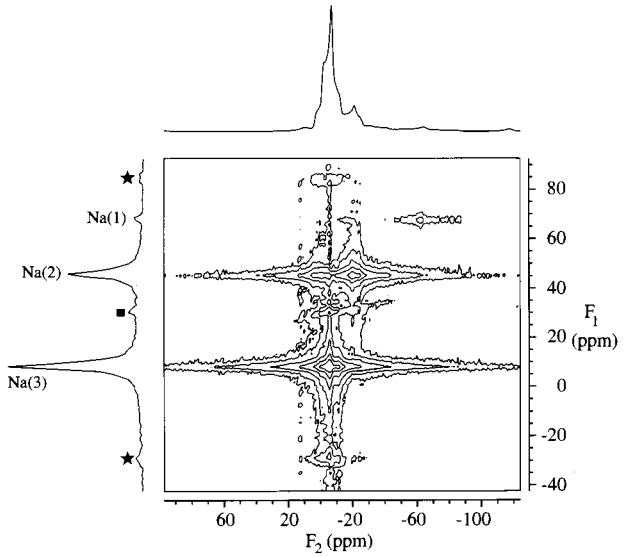

Figure 3. Contour plot of the ^{23}Na PFG-MQMAS spectrum (9.4 T) of $Na_5P_3O_{10}$ (phase II) obtained using the pulse scheme in Figure 2 with $\tau(\beta_1) = 1.8\ \mu s$, $\tau(\beta_2) = 17.6\ \mu s$, $G_1 = -17$ G/cm, $G_2 = 51$ G/cm, $\tau_g = 210\ \mu s$, and the fixed delay $\Delta = 260\ \mu s$. The spectrum was recorded with a spinning speed $\nu_r = 14.2$ kHz, a t_1 increment of 25 μs, and a total of 160 increments. For each increment, 500 scans were acquired with a repetition delay of 3 s. The solid square indicates a minor artifact in the spectrum resulting from single-quantum coherence which has not been completely dephased by the gradients while the asterisks indicate spinning sidebands in the F_1 dimension. The ^{23}Na MAS spectrum is shown at the top while the projection onto the F_1 dimension corresponds to a summation over the 2D spectrum. The contour lines are at levels of 1, 2, 4, 8, 16, and 32% of the maximum intensity. The spectrum is referenced to a 1.0 M aqueous solution of NaCl in both dimensions.

(II) listed in Table 1. The simulations employ intensity ratios of 1:2:2 for the three Na sites, where the largest quadrupole coupling corresponds to the low-intensity site, and they are observed to reproduce all spectral features of the experimental quadrupolar line shapes in Figure 4a and c. An independent test of the reliability of the C_Q, η_Q, and δ_{iso} values, obtained from the ^{23}Na MAS spectra, may be achieved by comparison of experimental and calculated isotropic 3Q shifts for a MQMAS experiment. For the $p = 0 \rightarrow -3 \rightarrow -1$ coherence transfer pathway observed in a MQMAS experiment of an $I = {}^3/_2$ nucleus, the isotropic 3Q shift ($\delta^{calc}_{iso,3Q}$) is given by eq 1[15,21]

$$\delta^{calc}_{iso,3Q} = \frac{17}{8}\delta_{iso} + \frac{1}{32}\frac{C_Q^2(1+\eta_Q^2/3)}{\nu_L^2} \times 10^6 \qquad (1)$$

where ν_L is the Larmor frequency. Employing the C_Q, η_Q, and δ_{iso} values for $Na_5P_3O_{10}$ (II) and eq 1 give the $\delta^{calc}_{iso,3Q}$ shifts listed in Table 1 which are observed to be in excellent agreement with the experimental isotropic 3Q shifts (Table 1), obtained from the MQMAS spectrum in Figure 3.

To date the largest ^{23}Na quadrupole coupling observed in a MQMAS NMR experiment has been reported for the Na(3) site of Na_2HPO_4 (i.e., $C_Q = 3.84$ MHz).[15,20,22,23] The quadrupole coupling of 4.57 MHz for the low-intensity site of $Na_5P_3O_{10}$ (II) is somewhat larger than this value. This may explain the low intensity for this site in the PFG-MQMAS spectrum (Figure 3) when the decrease in 3Q excitation and 3Q-to-1Q conversion efficiencies with increasing quadrupole coupling for the RIACT experiment[20] is taken into account. It may also account for the failure to observe this Na site in recent MQMAS investigations of $Na_5P_3O_{10}$,[15,16] especially in one of the investigations which was performed at a low magnetic field (4.7 T).[16] Table 1 also summarizes the recently reported C_Q, η_Q, and δ_{iso} values for the Na(2) and Na(3) sites of $Na_5P_3O_{10}$ (II). For site Na(3) these parameters are similar to those obtained in this work, while some discrepancies are observed for site Na(2).

The observation of three Na signals with relative intensities of 1:2:2 is in agreement with the reported crystal structure.[11]

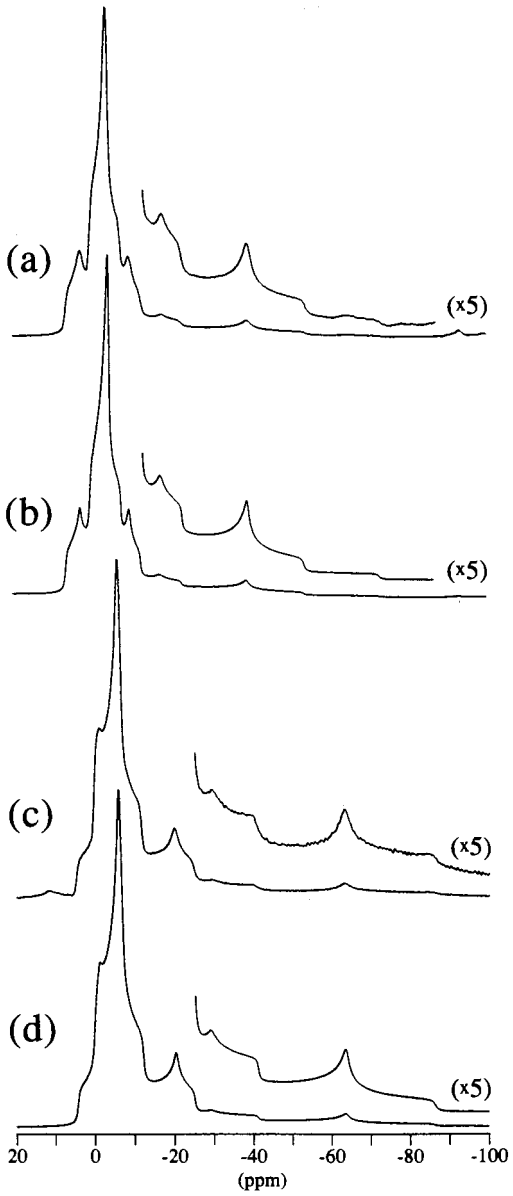

Figure 4. ^{23}Na MAS NMR spectra of the low temperature form of $Na_5P_3O_{10}$ (phase II) obtained at (a) 11.7 T and (c) 9.4 T using spinning speeds of 12.7 kHz and 13.3 kHz, respectively. 1190 scans with a repetition delay of 2 s were acquired for the 11.7-T spectrum while the spectrum at 9.4 T employed a 10 s repetition delay and 10,000 scans. Simulations of the central transitions at 11.7 and 9.4 T are shown in (b) and (d), respectively. The simulations use a 1:2:2 intensity ratio and the C_Q, η_Q, and δ_{iso} values listed in Table 1. The expansion of the low-frequency part of the overlapping central transitions illustrates spectral features which mainly originate from the low-intensity Na resonance (Na(1)) which has the largest quadrupole coupling.

(21) Massiot, D.; Touzo, B.; Trumeau, D.; Coutures, J. P.; Virlet, J.; Florian, P.; Grandinetti, P. J. *Solid State Nucl. Magn. Reson.* **1996**, *6*, 73.
(22) Baldus, M.; Meier, B. H.; Ernst, R. R.; Kentgens, A. P. M.; Meyer zu Altenschildesche, H.; Nesper, R. *J. Am. Chem. Soc.* **1995**, *117*, 5141.
(23) Wu, G.; Rovnyak, D.; Sun, B.; Griffin, G. *Chem. Phys. Lett.* **1995**, *249*, 210.

Table 1. ^{23}Na Quadrupole Coupling Constants (C_Q), Asymmetry Parameters (η_Q), and Isotropic Chemical Shifts (δ) for the Anhydrous $Na_5P_3O_{10}$ Polymorphs

	site[a]	occupancy	C_Q (MHz)	η_Q	δ_{iso} (ppm)[b]	$\delta^{obs}_{iso,3Q}$ (ppm)[c]	$\delta^{calc}_{iso,3Q}$ (ppm)[d]	ref
$Na_5P_3O_{10}$ (phase I)	Na(1)	1	1.30 ± 0.03	0.75 ± 0.05	6.5 ± 0.2	19.0 ± 0.5	19.4	*e*
	Na(2)/Na(3)	2	3.72 ± 0.04	0.17 ± 0.05	1.8 ± 0.4	} 40 ± 2	42.8	*e*
	Na(2)/Na(3)	2	3.62 ± 0.04	0.29 ± 0.04	0.9 ± 0.4	}	39.5	*e*
$Na_5P_3O_{10}$ (phase II)	Na(1)	1	4.57 ± 0.03	0.39 ± 0.02	3.5 ± 0.4	68.5 ± 0.5	68.7	*e*
	Na(2)	2	2.99 ± 0.02	0.19 ± 0.02	9.4 ± 0.2	45.8 ± 0.5	45.2	*e*
			1.75 ± 0.10	0.80 ± 0.20	−14.5 ± 1.0			15
			1.32 ± 0.01	0.81 ± 0.02	7.2 ± 0.4			16
	Na(3)	2	1.37 ± 0.02	1.00 ± 0.05	0.5 ± 0.2	8.7 ± 0.5	8.0	*e*
			1.40 ± 0.20	0.90 ± 0.20	−4.5 ± 2.0			15
			1.36 ± 0.02	1.00 ± 0.06	0.2 ± 0.9			16

[a] Assignment of the quadrupole coupling parameters to the different structural Na sites from the X-ray structure determinations (see text). [b] Isotropic chemical shift relative to an external 1.0 M aqueous solution of NaCl. [c] Isotropic triple-quantum shifts observed experimentally at 9.4 T. [d] Isotropic triple-quantum shifts at 9.4 T calculated from the C_Q, η_Q, and δ_{iso} values derived from simulations of the ^{23}Na MAS NMR experiments. [e] This work.

According to that study, all Na ions are octahedrally coordinated by oxygens and one Na atom (Na(1)) lies on a center of symmetry while the other two sites (Na(2) and Na(3)) occupy general positions. Thus, the low-intensity site, possessing the largest quadrupole coupling, originates from Na(1). The quadrupole couplings of the two other resonances are assigned to Na(2) and Na(3) from estimated quadrupole coupling constants (C_Q^{calc}) using point-monopole calculations[24] which only consider oxygen anions within the first coordination sphere of the ^{23}Na nucleus. The calculations employ effective oxygen charges (q_i) for the oxygen anions obtained from $q_i = (-2 + \Sigma f_{ij})e$, where f_{ij} is the covalence of the oxygen (i) − cation (j) bond calculated from the equations of Brown and Shannon[25] and the chemical bond data of Brown and Altermatt.[26] This method has recently proven successful for correlating structural geometries (i.e. C_Q^{calc}) with experimental quadrupole couplings for ^{23}Na in a series of sodium compounds[27] and for ^{133}Cs in various cesium salts.[28] Employing this method and using a ^{23}Na quadrupole moment $Q = 0.102 \times 10^{-28}$ m^2,[29] Sternheimer antishielding factor $\gamma_\infty = -4.56$,[30] and the structural data for $Na_5P_3O_{10}$ (II) from single-crystal XRD,[13] gives estimated quadrupole couplings of $C_Q^{calc} = 4.29$, 2.24, and 1.32 MHz for Na(1), Na(2), and Na(3), respectively. The C_Q^{calc} values agree favorably with those observed experimentally and yielding the assignment of the observed C_Q, η_Q, and δ_{iso} values to the three Na sites listed in Table 1.

^{23}Na MAS NMR spectra of the central transition for the high-temperature form of $Na_5P_3O_{10}$ (phase I) at 11.7 and 9.4 T are shown in Figure 5a and c, respectively. At first sight these spectra indicate the presence of two quadrupolar line shapes having an intensity ratio of 1:4. However, simulations using this assumption fail to give a satisfactory result for the apparent high-intensity second-order quadrupolar line shape observed in the region from about −5 to −75 ppm at 9.4 T. Furthermore, the high-frequency singularity of this quadrupolar line shape shows a slight splitting at 11.7 T due to the presence of two overlapping signals. This suggests that the total spectrum comprises three second-order quadrupolar line shapes with an intensity ratio of 1:2:2 where two of the line shapes have very similar C_Q, η_Q, and δ_{iso} values. Careful simulations of the spectra at both magnetic fields give the C_Q, η_Q, and δ_{iso} parameters listed in Table 1 for $Na_5P_3O_{10}$ (I). The optimized simulated spectra at 11.7 and 9.4 T, corresponding to these interaction parameters, are shown in Figure 5b and c, respectively, while Figure 5e and f illustrate separate simulations of the second-order quadrupolar line shapes for the high-intensity sites (Na(2) and Na(3)). The latter simulations and the parameters in Table 1 show that the main difference between these two line shapes is related to a variation in the asymmetry parameter.

Unfortunately, the small differences in C_Q, η_Q, and δ_{iso} values for Na(2) and Na(3) could not be confirmed by a MQMAS experiment (9.4 T) of $Na_5P_3O_{10}$ (I). This spectrum (not shown) displayed a 3Q resonance at 19 ppm from the Na(1) site and a second resonance at 40 ppm which was considerably broadened in the 3Q dimension. Calculation of the 3Q isotropic shifts at 9.4 T using eq 1 gives the values $\delta^{calc}_{iso,3Q} = 42.8$ ppm and $\delta^{calc}_{iso,3Q} = 39.5$ ppm for Na(2) and Na(3), respectively. The closeness of these shifts may partly account for the lack of resolution of these two sites in the MQMAS experiment taking into account that the digital resolution in the F_1 dimension was 1.7 ppm. Moreover, the quadrupolar line shapes observed for these two sites in the ^{23}Na MAS spectra (Figure 5) appear to be smeared out slightly which may indicate that our sample of $Na_5P_3O_{10}$ (I) is imperfectly crystalline. Several attempts were made to produce a $Na_5P_3O_{10}$ (I) sample of higher crystallinity using different heating/cooling temperatures and schemes but these failed to improve the resolution of the ^{23}Na quadrupolar line shapes for Na(2) and Na(3). The observation of disorder is not surprising since the high-temperature phase is obtained through a first-order solid−solid-phase transformation by heating the low-temperature form. This process involves considerable rearrangement of ions and thus might involve residual disorder.

The observation of three Na sites with relative intensities of 1:2:2 is in accordance with the relative multiplicities of Na(1), Na(2), and Na(3), respectively, in the crystal structure reported for $Na_5P_3O_{10}$ (I).[12] From the relative intensities it is clear that the low-intensity signal has to be assigned to site Na(1). This means that the high-intensity signal should arise from Na(2) and Na(3) with nearly identical C_Q, η_Q, and δ_{iso} values. These sites, however, are reported to have very different coordination environments: while Na(2) is in a distorted octahedral coordination with four short and two long Na−O contacts, Na(3) is in a 4-fold coordination with all oxygens being on one side of the cation. Calculation of the quadrupole coupling constants, using the point-monopole approach (vide supra) and the structural data reported for $Na_5P_3O_{10}$ (phase I),[12] gives values of $C_Q^{calc} = 2.44$,

(24) Cohen, M. H.; Reif, F. *Solid State Phys.* **1957**, *5*, 321.
(25) Brown, I. D.; Shannon, R. D. *Acta Crystallogr. A* **1973**, *29*, 266.
(26) Brown, I. D.; Altermatt, D. *Acta Crystallogr. B* **1985**, *41*, 244.
(27) Koller, H.; Engelhardt, G.; Kentgens, A. P. M.; Sauer, J. *J. Phys. Chem.* **1994**, *98*, 1544.
(28) Skibsted, J.; Vosegaard, T.; Bildsøe, H.; Jakobsen, H. J. *J. Phys. Chem.* **1996**, *100*, 14872.
(29) Lederer, M.; Shirley, V. S. *Table of Isotopes*, 7th ed.; Wiley-Interscience: New York, 1978.
(30) Sternheimer, R. M. *Phys. Rev.* **1959**, *115*, 1198.

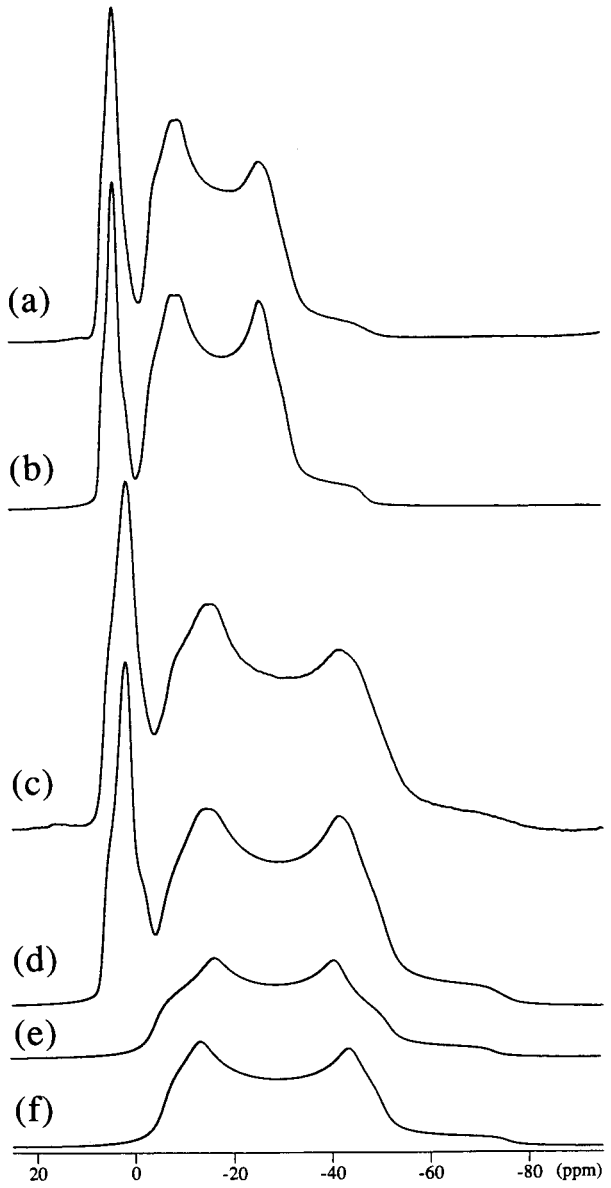

Figure 5. ^{23}Na MAS NMR spectra of the central transition for the high temperature form of $Na_5P_3O_{10}$ (phase I) at 11.7 T (a) and 9.4 T (c). Spinning speeds of 14.2 kHz and 12.0 kHz were employed and 3922 and 2700 scans were acquired for the 11.7- and 9.4-T spectra, respectively. Parts (b) and (d) illustrate simulations of the spectra in (a) and (c) using three overlapping quadrupolar line shapes with a 1:2:2 intensity ratio and the C_Q, η_Q, and δ_{iso} parameters summarized in Table 1. Separate simulations of the quadrupolar line shapes for the Na(3)/Na(2) sites are shown in (e) and (f) where part (e) corresponds to the resonance with the largest quadrupole coupling.

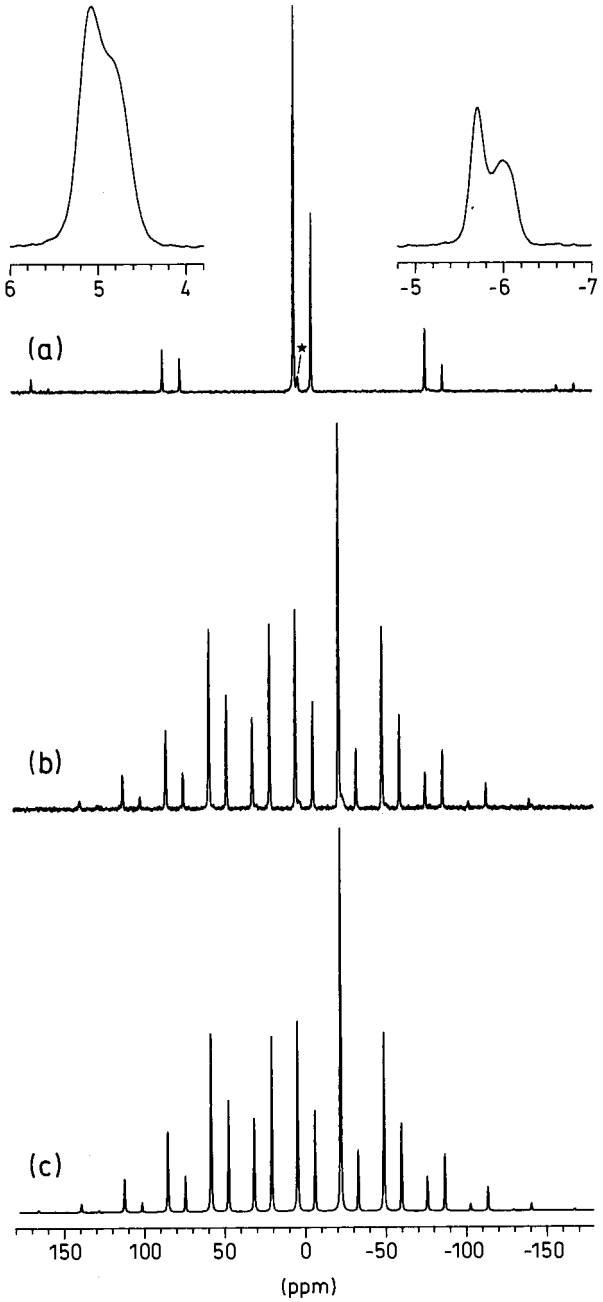

Figure 6. ^{31}P MAS NMR spectra (9.4 T) of the low temperature form of $Na_5P_3O_{10}$ (phase II) recorded using a repetition delay of 120 s and spinnings speeds of (a) $\nu_r = 13{,}185$ Hz (24 scans) and (b) $\nu_r = 4350$ Hz (30 scans). The asterisk in (a) indicates a resonance from a minor impurity phase while the insets illustrate the line shapes of the centerbands for the two ^{31}P sites. (c) Simulation of the spinning sideband intensities in (b) corresponding to the δ_σ, η_σ, and δ_{iso} values listed in Table 2 and a 1:2 intensity ratio.

3.30, and 2.87 MHz for Na(1), Na(2), and Na(3), respectively. These calculated values deviate significantly from those observed experimentally and do not allow for any assignment of the signals. Thus, apart from the straightforward distinction between Na(1) and Na(2)/Na(3) based on the relative intensities, no further interpretation of the ^{23}Na spectra is possible. It is unreasonable that the large differences in geometries for Na(2) and Na(3) should result in nearly identical quadrupole couplings for the two Na sites which suggests that the reported single-crystal structure for $Na_5P_3O_{10}$ (I) may be inaccurate in terms of the local Na environments.

^{31}P MAS NMR spectra (9.4 T) of $Na_5P_3O_{10}$ (II), recorded at two different spinning speeds, are shown in Figure 6a and b. The spectrum at highest spinning speed (Figure 6a) demonstrates the presence of two ^{31}P sites with relative intensities of 1:2 in agreement with the reported crystal structure[11] and with earlier ^{31}P MAS NMR observations.[31−33] The expansions of the centerbands in Figure 6a show that the individual resonances exhibit unique line shapes which apparently include two singularities. These line shapes may originate from homonuclear $^{31}P-^{31}P$ dipolar couplings, heteronuclear $^{31}P-^{23}Na$ dipolar

(31) Andrew, E. R.; Bryant, D. J.; Cashell, E. M.; Dunell, B. A. *Chem. Phys. Lett.* **1981**, *77*, 614.
(32) Burlinson, N. E.; Dunell, B. A.; Ripmeester, J. A. *J. Magn. Reson.* **1986**, *67*, 217.
(33) Hayashi, S.; Hayamizu, K. *Chem. Phys.* **1991**, 157, 381.

Table 2. ^{31}P Shielding Anisotropies (δ_σ), Asymmetry Parameters (η_σ), and Isotropic Chemical Shifts (δ_{iso}) for the Two $Na_5P_3O_{10}$ Polymorphs and for $Na_5P_3O_{10}\cdot 6H_2O$[a]

	site[b]	relative intensity	δ_σ[c] (ppm)	η_σ[c]	δ_{iso} (ppm)
$Na_5P_3O_{10}$	P(1)	1	116.1 ± 1.3	0.50 ± 0.03	-5.9 ± 0.2
(II)	P(2)	2	-107.4 ± 0.7	0.28 ± 0.02	5.0 ± 0.2
$Na_5P_3O_{10}$	P(1)	1	126.9 ± 1.7	0.45 ± 0.03	-7.5 ± 0.2
(I)	P(2)	2	-95.6 ± 1.3	0.27 ± 0.05	1.3 ± 0.1
$Na_5P_3O_{10}\cdot$	P(1)	1	-98.0 ± 3.8	0.00 ± 0.15	0.6 ± 0.3
$6H_2O$	P(2)	1	114.7 ± 1.8	0.51 ± 0.03	-6.7 ± 0.2
	P(3)	1	-100.5 ± 1.5	0.44 ± 0.05	2.8 ± 0.2

[a] Optimized data from least-squares fits to the integrated ssb intensities in ^{31}P MAS NMR spectra at 9.4 T. The error estimates are 95% confidence limits calculated for each parameter from the rms deviation between simulated and experimental ssb intensities using the procedure given in ref 28. [b] The numbering of the P sites is taken from the reported crystal structures.[10−14] For assignment, see text. [c] δ_σ and η_σ are defined by the principal elements (δ_{ii}) of the CSA tensor as $\delta_\sigma = \delta_{iso} - \delta_{33}$ and $\eta_\sigma = (\delta_{11} - \delta_{22})/\delta_\sigma$, where $\delta_{iso} = {}^1/_3\,(\delta_{11} + \delta_{22} + \delta_{33})$ and $|\delta_{33} - \delta_{iso}| \geq |\delta_{11} - \delta_{iso}| \geq |\delta_{22} - \delta_{iso}|$.

couplings and ^{31}P−^{31}P and/or ^{31}P−^{23}Na scalar *J*-couplings[34−38] because the high-field Hamiltonians for the CSA, quadrupolar, and dipolar coupling interactions have terms which do not commute with each other. As a result these effects are not completely removed by magic-angle spinning.[34] This phenomenom has partly been described for $Na_5P_3O_{10}$ (II) by Hayashi and Hayamizu,[33] who reported a small spinning-rate dependency (in the range $\nu_r = 1-5$ kHz) of the isotropic chemical shifts at 4.7 and 9.4 T as result of the simultaneous occurrence of ^{31}P CSA and ^{31}P−^{31}P dipolar couplings. However, these authors did not mention any effects from these interactions on the line shapes of the resonances. Unique powder line shapes of the centerband and spinning sidebands are also observed at lower spinning speeds. This fact and the relatively large difference in δ_{iso} values for the two ^{31}P resonances indicate that the line shapes are not a result of $n = 0$ rotational resonance dipolar recoupling; an effect which has been observed for chemically equivalent ^{31}P−^{31}P spin pairs.[39,40] The two manifolds of spinning sidebands, observed in the ^{31}P MAS NMR spectrum recorded at a lower spinning speed (Figure 6b), make it possible to determine the CSA parameters (δ_σ and η_σ) by least-squares optimization of simulated to experimental spinning sideband intensities. This gives the ^{31}P CSA parameters listed in Table 2 for $Na_5P_3O_{10}$ (II) and the simulated spectrum shown in Figure 6c. The CSA parameters and isotropic chemical shifts derived from Figure 6 are of slightly higher accuracy than those reported earlier for $Na_5P_3O_{10}$ (II).[32,33]

^{31}P MAS NMR studies of dipolar and *J*-coupled ^{31}P−^{31}P spin pairs have recently shown that these interactions can also be characterized from the intensities and line shapes of the spinning sidebands in slow-speed MAS NMR spectra.[36−38] Furthermore, it has been shown that a reliable analysis of the spinning sideband intensities requires consideration of at least the direct ^{31}P−^{31}P dipolar interaction, in addition to the chemical shielding anisotropy, in cases where the CSA interaction is small and where the ^{31}P−^{31}P dipolar interaction is of a comparable magnitude to the spinning speed.[36] The analysis in this work only includes the effect from the chemical shielding anisotropy and extracts the CSA parameters from least-squares fitting to integrated spinning sideband intensities. This is expected to be an acceptable approximation for the $Na_5P_3O_{10}$ polymorphs because the shielding anisotropies for the individual sites are relatively large and the lowest spinning speeds employed for the experimental spectra ($\nu_r = 4.4$ kHz) are about a factor of 5 larger than the strongest ^{31}P−^{31}P dipolar interaction; the calculated ^{31}P−^{31}P dipolar coupling constant, $R = \mu_0 h(\gamma_P)^2/(16\pi^3 r_{P,P}^3)$, is 848 Hz for the ^{31}P(1)−^{31}P(2) dipolar coupling in $Na_5P_3O_{10}$ (II). There is thus expected to a negligible effect of ^{31}P−^{31}P dipolar couplings on the spinning sideband intensities.

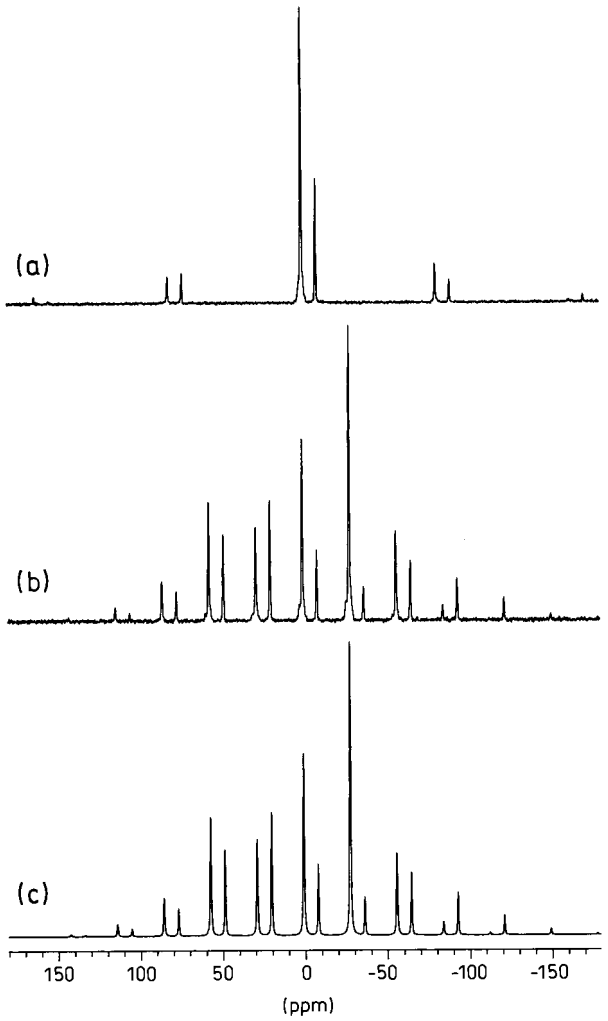

Figure 7. ^{31}P MAS NMR spectra (9.4 T) of the high-temperature polymorph of $Na_5P_3O_{10}$ (phase I) recorded using a 120 s repetition delay and (a) $\nu_r = 13\,115$ Hz (30 scans) and (b) $\nu_r = 4580$ Hz (48 scans). A spinning sideband manifold from a minor impurity phase is observed at the high-frequency side of the spinning sideband manifold from the P(2) resonance (i.e. $\delta_{iso} = 1.3$ ppm). The simulation of the spectrum obtained with $\nu_r = 4580$ Hz shown in (c) employs an 1:2 intensity ratio and the optimized δ_{iso} and CSA parameters in Table 2.

The ^{31}P MAS NMR spectra of the high-temperature form, shown in Figure 7a and b, also reveal two ^{31}P sites in the ratio 1:2 in agreement with the crystal structure of $Na_5P_3O_{10}$ (I).[12] However, for this sample unique line shapes of the centerbands and spinning sideband are not resolved which we tentatively ascribe to a lower degree of crystallinity for this sample compared to the low-temperature form, consistent with the interpretation of the ^{23}Na MAS NMR data (vide supra). The

(34) Maricq, M. M.; Waugh, J. S. *J. Chem. Phys.* **1979**, *70*, 3300.
(35) Olivieri, A. C. *J. Magn. Reson.* **1989**, *81*, 201.
(36) Wu, G.; Wasylishen, R. E. *J. Chem. Phys.* **1993**, *99*, 6321.
(37) Eichele, K.; Wasylishen, R. E. *J. Phys. Chem.* **1994**, *98*, 3108.
(38) Wu, G.; Sun, B.; Wasylishen, R. E.; Griffin, R. G. *J. Magn. Reson.* **1997**, *124*, 366.
(39) Kubo, A.; McDowell, C. A. *J. Chem. Phys.* **1990**, 92, 7156.
(40) Dusold, S.; Klaus, E.; Sebald, A.; Bak, M.; Nielsen, N. C. *J. Am. Chem. Soc.* **1997**, *119*, 7121.

line widths of the ^{31}P resonances in Figure 7a (fwhm(P1) = 0.66 ppm and fwhm(P2) = 0.62 ppm) are slightly larger than those observed for the low-temperature form (fwhm(P1)= 0.57 ppm and fwhm(P2)= 0.50 ppm, Figure 6a). Least-squares optimization of the spinning sideband intensities from the spectrum at low spinning speed (Figure 7b) gives the CSA parameters listed in Table 2 for $Na_5P_3O_{10}$ (I) and the simulation shown in Figure 7c. These parameters deviate only slightly from those obtained for the low-temperature polymorph, indicating that only minor changes in the geometry of the $P_3O_{10}^{5-}$ ion occur during the phase transition. Furthermore, it is seen that the terminal P atoms of the $P_3O_{10}^{5-}$ units have a negative shielding anisotropy parameter (δ_σ), demonstrating that the unique principal element of the CSA tensor (δ_{33}) is the least-shielded principal element of the CSA tensor when the definition $|\delta_{33} - \delta_{iso}| \geq |\delta_{11} - \delta_{iso}| \geq |\delta_{22} - \delta_{iso}|$ is used. Similar observations have been reported from ^{31}P NMR investigations of diphosphates,[33,41−43] for which the δ_{33} elements are always the least shielded principal CSA tensor element. ^{31}P single-crystal NMR of α-$Ca_2P_2O_7$ has shown that the least-shielded principal element of the CSA tensor lies along the direction of the P−O(−P) bond[41] which is longer than the remaining three P−O contacts. Similar geometries have been reported for the terminal PO_4^{3-} units of the $P_3O_{10}^{5-}$ ions in the $Na_5P_3O_{10}$ polymorphs[11,12] and thus, it is expected that the δ_{33} elements of the CSA tensors for these sites are lying in the approximate direction of the P−O(−P) bond.

The above information may be used in the assignment of the three ^{31}P resonances observed in the ^{31}P MAS NMR spectra of $Na_5P_3O_{10}\cdot 6H_2O$ shown in Figure 8. The expansion of the centerbands in the spectrum at high spinning speed (Figure 8a) demonstrates that two of the resonances exhibit unique line shapes, as a result of homo- and/or heteronuclear dipolar couplings, while the third site has a broader featureless line shape. The observation of three resonances with approximately equal intensities is in accord with the crystal structure reported for the hexahydrate[14] which reveals three ^{31}P sites with equal occupancies. CSA parameters for the three ^{31}P sites can be extracted from simulations of the spinning sideband intensities in the spectrum at lower spinning speed (Figure 8b) and are listed along with the isotropic chemical shifts in Table 2. According to the above discussion, the ^{31}P resonances exhibiting a negative δ_σ are assigned to the terminal P atoms of the $P_3O_{10}^{5-}$ ion (e.g. P(1) and P(3) in the reported crystal structure). This assignment is supported by a comparison of the δ_{iso} values for $Na_5P_3O_{10}\cdot 6H_2O$ with those for the anhydrous polymorphs in that all terminal P atoms have values that are 7−10 ppm lower than those of the middle P sites. The broadening of the resonance at 0.6 ppm strongly depends on the spinning speed and is ascribed to insufficient averaging of $^1H-^{31}P$ dipolar couplings by MAS for this resonance. The PO_4 tetahedron of the P(1) site participates in nine hydrogen bonds while the other terminal unit (P(3)) only takes part in one. Thus, we tentatively assign the broadened resonance (δ_{iso} = 0.6 ppm) to the P(1) site, leading to the complete assignment of all three resonances given in Table 2.

Finally, we note that preliminary ^{23}Na MAS and MQMAS investigations have also been performed for the hexahydrate. The ^{23}Na MAS NMR spectrum of this phase is considerably more complex than the corresponding spectra of the anhydrous polymorphs since it is composed of second-order quadrupolar line shapes originating from five different Na sites. However, the hexahydrate can easily be distinguished from the anhydrous forms on basis of ^{23}Na MAS NMR. A complete analysis for the hexahydrate, involving ^{23}Na MAS and MQMAS NMR spectra recorded at different magnetic fields, is currently in progress.

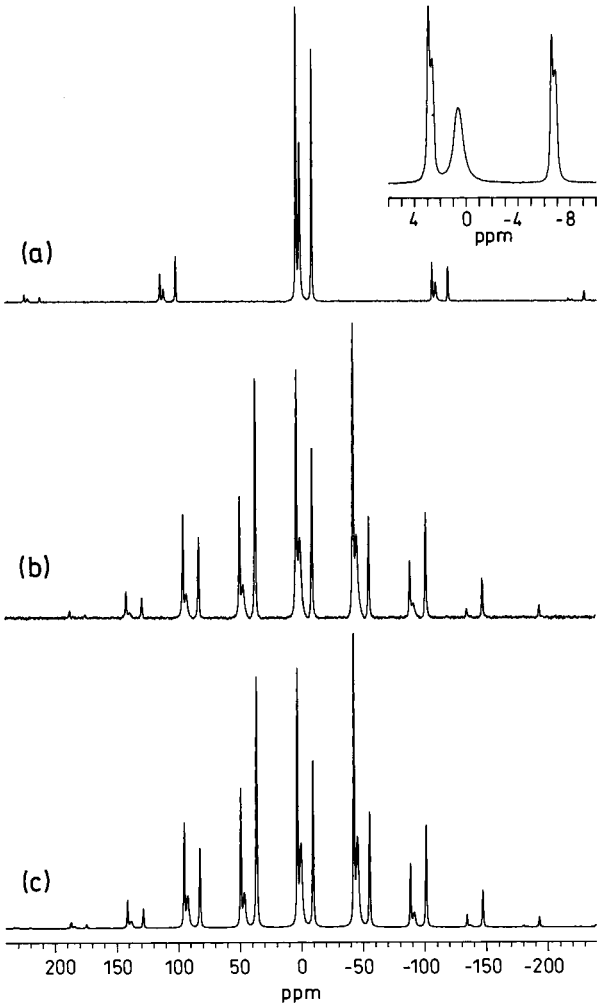

Figure 8. ^{31}P MAS NMR spectra (9.4 T) illustrating the spinning sideband manifolds for the three ^{31}P sites in $Na_5P_3O_{10}\cdot 6H_2O$ at spinning speeds of 13 340 Hz (a) and 5,575 Hz (b). The spectrum in (a) employed a repetition delay of 60 and 80 scans while the spectrum in (b) used a 30-s repetition delay and 193 scans. The inset in (a) illustrates that unique powder line shapes are observed for two of the ^{31}P resonances (δ_{iso} = 2.8 ppm and δ_{iso} = −6.7 ppm) while the third ^{31}P resonance (δ_{iso} = 0.6 ppm) has a somewhat broader and featureless line shape. (c) Simulation of the spinning sideband intensities in (b) corresponding to the δ_{iso} and CSA parameters listed in Table 2. The intensity ratio and the linebroadening of the individual spinning sideband patterns were adjusted to give the best fit to the experimental spectrum.

Conclusions

Parameters for the ^{23}Na quadrupole couplings and isotropic chemical shifts have been accurately determined for the three crystallographically distinct Na sites in both anhydrous polymorphs of $Na_5P_3O_{10}$ using ^{23}Na MAS NMR and the pulsed field gradient MQMAS technique. For the low-temperature form these results clarify discrepancies between recent MQMAS NMR studies and the crystal structure reported from X-ray diffraction. Furthermore, the MQMAS spectrum of this phase

(41) Kohler, S. J., Ellett, J. D.; Klein, M. P. *J. Chem. Phys.* **1976**, *64*, 4451.
(42) Duncan, T. M.; Douglass, D. C. *Chem. Phys.* **1984**, *87*, 339.
(43) Hartmann, P.; Vogel, J.; Schnabel, B. *J. Magn. Reson. Ser. A.* **1994**, *111*, 110.
(44) Frydman, L.; Harwood, J. S. *J. Am. Chem. Soc.* **1995**, *117*, 5367.

includes the observation of the largest ^{23}Na quadrupole coupling ($C_Q = 4.57$ MHz) reported to date by MQMAS NMR. The ^{23}Na quadrupole coupling parameters have allowed an assignment of the individual resonances to the three different Na sites in the crystal structure of the low-temperature form. The ^{23}Na NMR data for the high temperature form indicate inaccuracies in the crystal structure reported for this phase.

The ^{31}P chemical shielding data, obtained from ^{31}P MAS NMR spectra of the anhydrous polymorphs, show negative shielding anisotropy parameters ($\delta_\sigma = \delta_{iso} - \delta_{33}$) for the terminal P atoms of the $P_3O_{10}^{5-}$ ions in agreement with earlier observations for diphosphates. This characteristic feature has been applied in the assignment of the three ^{31}P resonances observed for the hexahydrate $Na_5P_3O_{10}\cdot 6H_2O$. In conclusion, the present study exemplifies the power of solid-state NMR in structural investigations of different crystalline forms of a compound (e.g. polymorphs or hydrates) and its great sensitivity to local structural details.

Acknowledgment. We acknowledge the financial assistance of the NSERC of Canada in form of operating and equipment grants (C.A.F.). J.S. thanks the Danish Natural Research Council (J. No. 9600396) for financial support.

IC980524O